Journal of Physics: Materials

CrossMark

OPEN ACCESS

RECEIVED
5 August 2022

REVISED
24 October 2022

ACCEPTED FOR PUBLICATION
2 November 2022

PUBLISHED
14 November 2022

PAPER

Advanced characterization of organic–metal and organic–organic interfaces: from photoelectron spectroscopy data to energy-level diagrams

Qi Wang[1,2,3], **Jiacheng Yang**[1], **Alexander Gerlach**[3], **Frank Schreiber**[3] and **Steffen Duhm**[1,2,*]

[1] Institute of Functional Nano and Soft Materials (FUNSOM), Joint International Research Laboratory of Carbon-Based Functional Materials and Devices, Soochow University, Suzhou 215123, People's Republic of China
[2] Jiangsu Key Laboratory of Advanced Negative Carbon Technologies, Soochow University, Suzhou 215123, People's Republic of China
[3] Institut für Angewandte Physik, Universität Tübingen, 72076 Tübingen, Germany
[*] Author to whom any correspondence should be addressed.

E-mail: duhm@suda.edu.cn

Keywords: organic heterostructure, energy-level alignment, photoelectron spectroscopy, organic–inorganic interface, phthalocyanine, chemisorption, physisorption

Supplementary material for this article is available online

Abstract

Organic–metal and organic–organic interfaces account for the functionality of virtually all organic optoelectronic applications and the energy-level alignment is of particular importance for device performance. Often the energy-level alignment is simply estimated by metal work functions and ionization energies and electron affinities of the organic materials. However, various interfacial effects such as push back, mirror forces (also known as screening), electronic polarization or charge transfer affect the energy-level alignment. We perform x-ray and ultraviolet photoelectron spectroscopy (XPS and UPS) measurements on copper-hexadecafluorophthalocyanine ($F_{16}CuPc$) and titanyl-phthalocyanine (TiOPc) thin films on Ag(111) and use TiOPc bilayers to decouple $F_{16}CuPc$ layers from the metal substrate. Even for our structurally well-characterized model interfaces and by stepwise preparation of vacuum-sublimed samples, a precise assignment of vacuum-level and energy-level shifts remains challenging. Nevertheless, our results provide guidelines for the interpretation of XPS and UPS data of organic–metal and organic–organic interfaces.

1. Introduction

The functionality of virtually all organic and hybrid (opto-)electronic devices depends on interface energetics, and a thorough understanding of energy-level alignment mechanisms at organic–metal and organic–organic interfaces is indispensable for further efficiency improvements [1–5]. For example, the energy-level offset at the donor–acceptor interface in organic photovoltaic devices is crucial for exciton dissociation [6–8]; chemisorbed molecular monolayers on metals can tune the substrate work functions by an interfacial charge transfer [9, 10] and allow, consequently, to lower charge injection barriers into electrodes [11, 12]. The number of organic materials used for optoelectronic applications is virtually unlimited [13, 14] and energy-level diagrams (ELDs) are frequently used to choose the best material for a given purpose [4, 15]. The energy values such as the ionization energies (IEs) for these ELDs are often taken from ultraviolet photoelectron spectroscopy (UPS) measurements [16, 17]. However, IEs depend, e.g. on the supramolecular organization of the thin film, the layer thickness and possible substrate–adsorbate interaction [18–21]. Furthermore, in UPS data of organic ultrathin films on metals spectral signatures from molecular valence levels overlap with these of the substrate, typically the metal d-bands, which makes it difficult to track thickness-dependent energy-level shifts [9, 18]. This obstacle can be tackled by estimating the position of valence levels via core level measurements by x-ray photoelectron spectroscopy (XPS), as was already shown in the 80s for inorganic semiconductors [22, 23]. Moreover, XPS has elemental sensitivity and

gives insight into the chemical states of adsorbate atoms via so-called chemical shifts [24, 25]. Our focus issue article highlights that, in order to get a full picture of organic–metal and organic–organic interface energetics, advanced characterization by photoelectron spectroscopy—including UPS and XPS—is mandatory.

We start with a short introduction to photoelectron spectroscopy at these interfaces. UPS and XPS are both surface sensitive techniques and for organic materials (and measurements with typical lab light-sources like HeI and Al Kα) the mean free path of photoelectrons, i.e. the information depth, is around 5–10 Å for UPS and 50–100 Å for XPS [26, 27]. This applies for valence levels like the highest occupied molecular orbital (HOMO)-level (measured by UPS) and for core levels like the C 1s level (measured by XPS). Furthermore, the low kinetic secondary electron cutoff (SECO) of UPS allows to measure the *surface* potential of the sample, which is usually referred to as vacuum level (VL) [28, 29]. It becomes apparent that these different information depths are a challenge for the analysis of photoelectron spectra, especially for inhomogeneous samples [30, 31] and in case of energy-level bending, i.e. the parallel shift of VL, valence and core levels as function of layer thickness [32–34]. The chemical shift of the C 1s core level between carbon atoms in the conjugated backbone and in the functional groups of an organic molecule allows to assign spectral signatures to a specific layer in an organic heterostructure [9, 18]. Noteworthy, chemical shifts can be rather small [35, 36] and require high energy-resolution XPS data, i.e. measurements with a monochromatized x-ray source or at a synchrotron radiation facility. Furthermore, XPS allows to estimate the coupling strength at organic–metal interfaces as chemisorption, i.e. the re-hybridization of the molecular adsorbate in the contact layer [37, 38], leads to additional chemical shifts [10, 39].

Here, we aim to give guidelines for extracting meaningful energy levels from photoelectron spectroscopy data by taking several interface phenomena into account. In particular, we focus on the push-back effect, the image-charge effect ('screening') and possible charge transfer at the organic–metal interface [18] and at polarization effects (induction and electrostatic), possible intermolecular interaction and dipole layers at the organic–organic interface [40, 41]. Notably, the latter effects can also occur at organic–organic homointerfaces and the complex situation is illustrated in figure 1 by schematic ELDs of molecular thin films on clean metal surfaces. In both panels, the Fermi-level (E_F) and the work function (ϕ) are shown for the metal substrate. For each of the molecular layers (MLs), the VL, the lowest unoccupied molecular orbital (LUMO)-level, the HOMO-level, the carbon core level (C 1s) and a core level of a heteroatom (HA) are shown. Figure 1(a) shows four layers of a chemisorbed, non-polar molecule and figure 1(b) two layers of the same molecule on a spacer comprising two layers of a polar molecule. The VL, and the binding energy (BE) positions of valence and core levels at these interfaces are affected by:

(1) The push-back effect decreases the VL at both interfaces (figures 1(a) and (b)) upon deposition of the contact layer (1 ML) [5, 42].
(2) The bond dipole increases the VL due to interfacial charge transfer at the chemisorptive interface (figure 1(a)) [39, 43].
(3) The p_z-component of the dipole layers impacts the VL and the energy levels due to molecular dipole moments [44, 45]. In the contact layer (1 ML) of figure 1(b) only the HA of the molecule is located above this dipole layer and, consequently, also only the HA energy level is affected by the dipole layer; in the second layer (2 ML) the molecular dipole moments cancel each other [40].
(4) The screening effect (also called image-charge effect) affects the BE positions of unoccupied and occupied energy levels between the monolayer and the bilayer and leads to a decrease of the molecular energy gap in the contact layer at both interfaces (figures 1(a) and (b)) [46, 47].
(5) Chemisorption (figure 1(a)) leads to energy-level shifts in the contact layer [38, 39]. As chemisorption often goes along with a charge transfer, these energy-level shifts are related to the VL-shifts caused by effect #2.
(6) Polarization effects lead to energy-level shifts at each organic–organic interface [48–50]. For the sake of clarity, only the impact on the third ML by deposition of the fourth ML is shown in figures 1(a) and (b). The polarization can be divided into two contributions: (1) the induction contribution depends mainly on the dielectric constant of the MLs and (2) the electrostatic contribution takes also the molecular quadrupole moments into account [41].

This list and the ELDs in figure 1 are rather simplified as the interface phenomena leading to the shifts are correlated to each other. However, a detailed description of the physical mechanisms leading to shifts of VL and energy levels at these organic–metal and organic–organic interfaces is beyond the scope of this article and the reader is referred to the references, e.g. to the comprehensive review article 'The Impact of Dipolar Layers on the Electronic Properties of Organic/Inorganic Hybrid Interfaces' by Zojer *et al* [40]. Furthermore, for all layers in figure 1 (with the exception of the chemisorbed monolayer), E_F is rather at mid-gap position and energy-level and VL-shifts due to Fermi-level pinning at the frontier molecular orbitals and/or gap states

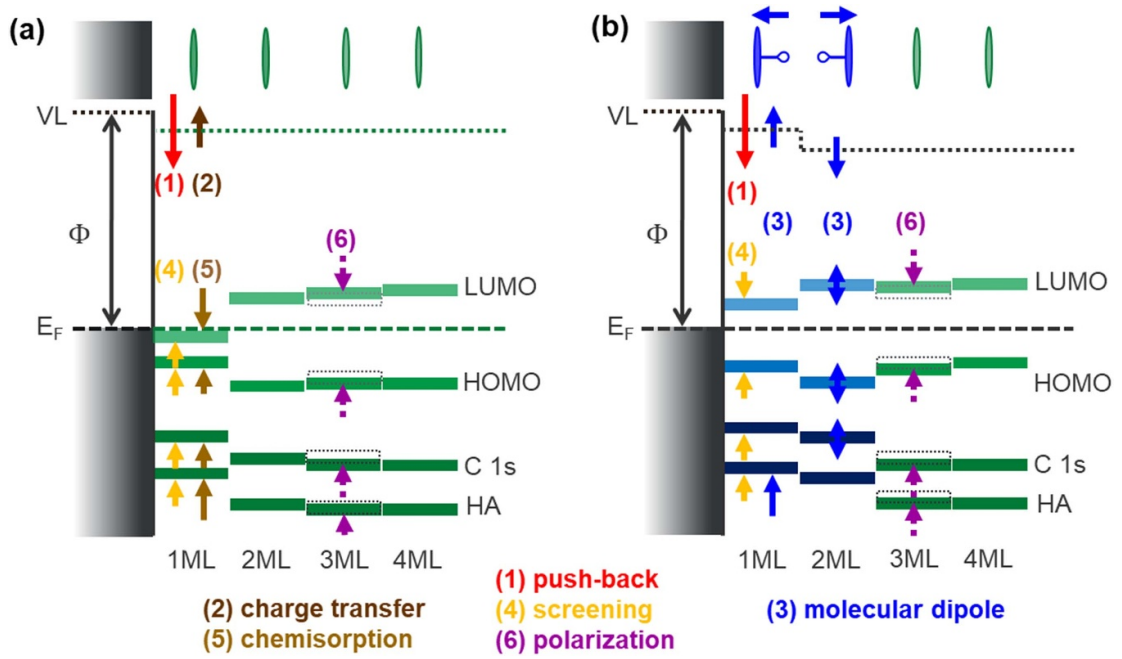

Figure 1. Schematic ELDs of organic–metal and organic–organic interfaces. The metal substrate is characterized by its work function (ϕ), i.e. the energetic difference between the Fermi-level (E_F) and the VL. For each ML the LUMO- and the HOMO-levels, the C 1s core level and the core level of a HA are shown. The arrows show VL and energy-level shifts upon deposition of the respective layer. For the sake of clarity, the polarization effects at the organic–organic interfaces are only shown for 3 ML; full bars depict the energy levels before and dotted bars after deposition of 4 ML. (a) The contact layer (1 ML) is chemisorbed involving a partial filling of the F-LUMO. (b) The contact layer is physisorbed; the p_z-components of the polar molecules in 1 ML and 2 ML are antiparallel.

[51–54] are not considered. Noteworthy, the density of gap or tailing states is usually too low to be detected with conventional UPS-setups [55, 56]. Nevertheless, they provide a charge reservoir for electronic-equilibrium-driven interfacial charge transfer, which typically leads to energy-level bending over a few organic layers [51, 52]. In contrast, a charge transfer by chemisorption leads to an interface dipole, i.e. an abrupt change of VL at the organic–metal interface [9, 18]. Noteworthy, the effects mentioned above impact the position of energy levels and further effects impact the line shape and intensities of UPS and XPS spectra, they include energy dispersion [27, 57, 58], orbital delocalization [59, 60], hole–phonon coupling [61, 62], photoelectron angular distribution [63–65], photoelectron diffraction [66, 67], core-hole screening [68–70] and shake-up excitations [71, 72]. Several tutorial-like review articles give guidelines how to analyze XPS data [73–75]; for UPS the reader is referred to these books [76, 77].

To model the organic–metal and organic–organic interfaces of figure 1, phthalocyanine-derivatives are chosen because they allow simple replacement of central atoms and further functionalization by molecular side groups [78, 79]. We use titanyl-phthalocyanine (TiOPc) as the bottom layer of the heterostructure: the intrinsic dipole moments of TiOPc have an antiparallel orientation in the first and second layer on Ag(111) with layer-by-layer growth and thereby provide a stable, weakly interacting contact layer [80–83]. Furthermore, homogeneous and well-ordered bilayers can be prepared by thermal desorption of multilayers and bilayer formation can be evidenced by XPS [84]. The TiOPc bilayer thickness of ∼6.3 Å [80] should be sufficient to shield the metal substrate from the second organic layer (i.e. the one above the TiOPc bilayer) and to facilitate a true organic–organic interface. We use copper-hexadecafluorophthalocyanine ($F_{16}CuPc$) as the second layer: fluorine functionalization adds an additional core level for XPS investigation and prevents undesired molecular diffusion [85]. Furthermore, fluorination of conjugated molecules leads to interesting and partially unexplained thickness-dependent energy-level shifts [86–89]. Overall, we perform thickness-dependent UPS and XPS measurements of TiOPc and $F_{16}CuPc$ (chemical structures in figure 2) deposited on Ag(111) and compare the results with $F_{16}CuPc$/bilayer TiOPc/Ag(111) heterostructures. Our photoelectron spectroscopy data show that all the effects mentioned above and highlighted in figure 1 occur at these structurally well-defined interfaces. Therefore, they serve as model systems for the advanced characterization of organic–metal and organic–organic interfaces by UPS and XPS using lab-based monochromatized UV and x-ray light sources.

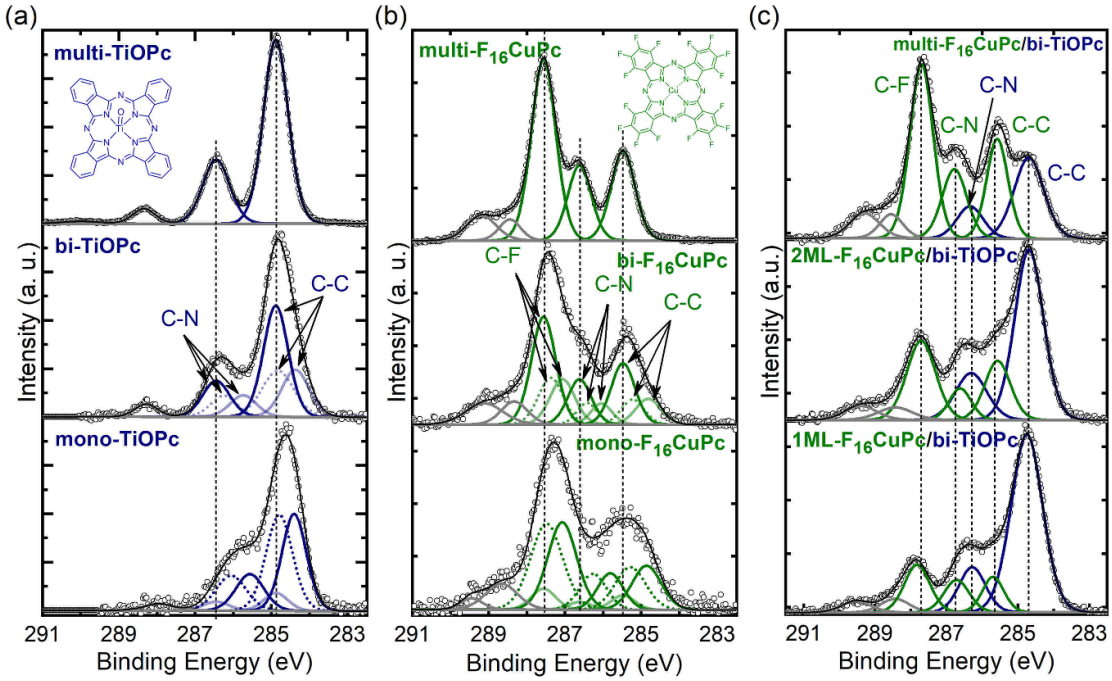

Figure 2. C 1s core level spectra and fits for organic thin films on Ag(111). The insets show the molecular structures of TiOPc and F_{16}CuPc. (a) TiOPc layers with thicknesses of 4 Å (mono-TiOPc), 8 Å (bi-TiOPc) and 64 Å (multi-TiOPc). (b) Spectra with the same thicknesses of F_{16}CuPc on Ag(111). (c) Stepwise deposited F_{16}CuPc layers on a nominal TiOPc bilayer (prepared by desorption of multilayers). The TiOPc and F_{16}CuPc contributions to the spectra are color-coded and the gray curves correspond to shake-up satellites.

2. Experimental methods

Thickness-dependent UPS and XPS measurements were carried out in an ultra-high vacuum system consisting of three interconnected chambers: an evaporation chamber (base pressure: 3×10^{-10} mbar), an annealing and sputtering chamber (3×10^{-10} mbar) and an analysis chamber (base pressure: 2×10^{-10} mbar). Ag(111) was cleaned by several cycles of Ar^+ ion bombardment and annealing (400 °C–500 °C). F_{16}CuPc and TiOPc were sublimated by physical vapor deposition from resistively heated cells with deposition rates of ~0.2 Å min^{-1}. The mass-related thickness was monitored by a quartz-crystal microbalance (QCM) positioned near the sample. In general, for phthalocyanines with a lying adsorption geometry a mass thickness of around 4 Å corresponds to nominal monolayer coverage [18]. UPS experiments were performed using monochromatized He I radiation (21.22 eV) and a SPECS PHOIBOS 150 analyzer. The energy resolution was 80 meV. The angle between the incident beam and the sample was fixed to 40°. The spectra were collected at photoelectron take-off angles of 45° with an acceptance angle of ±12° along the <11–2> azimuthal direction of Ag(111). A sketch of the measurement geometry can be found in [90]. The SECO (to determine the VL) was measured in normal emission with a bias potential of −3 V. XPS was performed using a monochromatized Al Kα source (1486.6 eV). The data analysis was carried out by a nonlinear least-square fitting routine, using Gaussian/Lorentzian peak shapes and a Shirley background. The error bar for the BEs is estimated to be ±0.05 eV. All measurements have been performed at room temperature (295 K).

3. Experimental results

The C 1s XPS data of the single-component systems and the heterostructure are shown in figure 2. The spectrum of TiOPc in multilayers (QCM thickness: 64 Å) on Ag(111) (top panel of figure 2(a)) is in accordance with literature data [84]. The three distinct peaks can be assigned to carbon atoms bound to another carbon atom (C–C), centered at 284.90 eV BE, carbon atoms bound to a nitrogen atom (C–N), centered at 286.45 eV BE, and a shake-up satellite, centered at 288.35 eV BE. In the spectrum of the nominal TiOPc bilayer (QCM thickness: 8 Å) (figure 2(b), middle panel) the C–C and C–N peaks are substantially broadened, which is due to monolayer contributions to the spectrum (the information depth of XPS is much larger than the overall film thickness). To fit this spectrum, the BEs of the C–C and C–N peaks are fixed at their multilayer positions and the four additional peaks, which are necessary to get a good fit, stem from

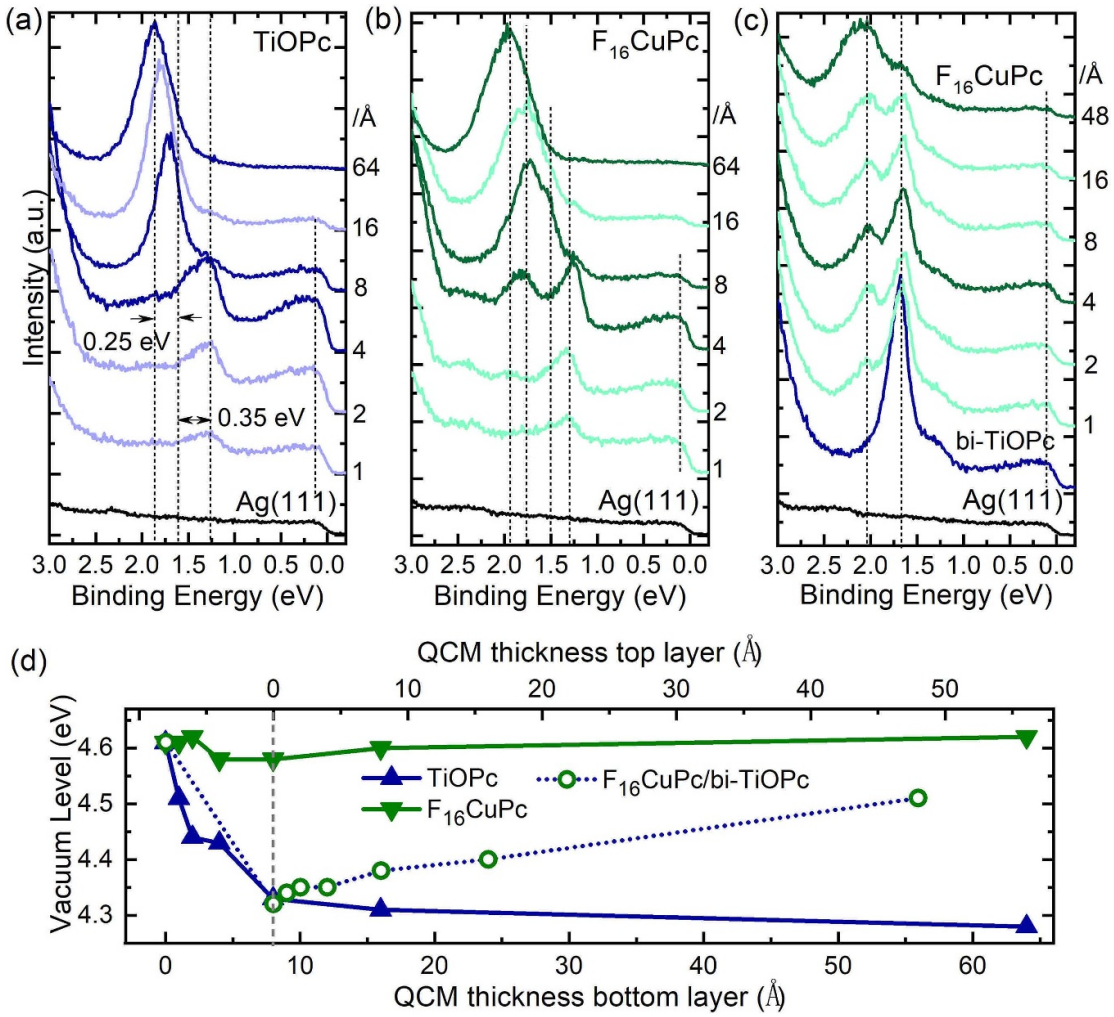

Figure 3. UPS data of stepwise deposited thin films of (a) TiOPc, (b) $F_{16}CuPc$ on Ag(111) and (c) $F_{16}CuPc$ on a nominal bilayer TiOPc on Ag(111). The spectra with a nominal monolayer, bilayer and multilayer coverage are highlighted by darker lines. (d) Thickness-dependent evolution of the VL w.r.t. the Fermi-level for all investigated thin films on Ag(111).

TiOPc in the contact layer. The C 1s spectrum of the nominal TiOPc bilayer prepared by stepwise deposition is rather similar to that of TiOPc prepared by multilayer desorption (figure S1), which shows that a thickness of 8 Å corresponds, indeed, to bilayer coverage. Furthermore, the multilayer contribution to the spectrum of the nominal monolayer (QCM thickness: 4 Å) (figure 2(a), bottom panel) is rather weak, which shows that the first two layers of vacuum-sublimed TiOPc on Ag(111) grow almost layer-by-layer. Before discussing the reasons for the doubled monolayer contributions, we turn to $F_{16}CuPc$ on Ag(111). In the spectrum with multilayer coverage (top panel of figure 2(b)), in addition to C–C and C–N, C–F is apparent and the spectrum is almost identical to the multilayer spectra on other substrates [91]. The spectrum of nominal $F_{16}CuPc$ bilayer coverage (middle panel of figure 2(b)) exhibits multilayer and monolayer features and the latter features are dominating the spectrum with nominal monolayer coverage (bottom panel of figure 2(b)).

The C 1s spectrum of the nominal $F_{16}CuPc$ monolayer on Ag(111) is virtually identical to a previously published spectrum of the same sample [68]. In this publication, Borghetti *et al* used near-edge x-ray absorption spectroscopy and UPS to show that the doubled core levels are due to a lifted degeneracy of the LUMO-level upon partial charging in combination with core-hole screening effects. Following these arguments, we used two sets of monolayer peaks with the same intensity to get the fitting results in figure 2(b). Furthermore, also our UPS results show a partially filled former LUMO (F-LUMO) for the $F_{16}CuPc$ monolayer on Ag(111) (figure 3(b)). Likewise, also the LUMO of TiOPc gets partially filled in the monolayer (figure 3(a)) and the C 1s core level spectrum of the TiOPc monolayer (figure 2(a)) can be fitted in an analogous way to the $F_{16}CuPc$ monolayer. All shifts of the C 1s components as well as N 1s and F 1s (figure S2) are summarized in table S1 and will be discussed further below. In the heterostructures (figure 2(c)), the C–F component of $F_{16}CuPc$ is well separated from the TiOPc features and shifts by ~0.1 eV to lower BE by increasing the $F_{16}CuPc$ coverage from monolayer (bottom panel) to multilayer (top panel).

The C–C component shifts in parallel, while the C–N component shifts slightly to higher BE. However, as these components overlap with the TiOPc features, their BE positions are not as reliable as those of C–F.

The valence UPS data of TiOPc on Ag(111) (figure 3(a)) are virtually identical to previous data [80, 84]: for nominal monolayer coverage, the HOMO-derived peak is centered at 1.27 eV BE, and a peak near the Fermi edge is assigned to the F-LUMO, which becomes partially populated by charge transfer from the substrate. For nominal bilayer coverage, the intensities of the F-LUMO and the HOMO peaks decrease while a peak centered at 1.62 eV BE emerges, which is attributed to the second layer and shows a further shift by increasing the coverage to multilayers. The VL (as derived from the SECOs, figure S3) decreases by 0.32 eV until bilayer coverage is reached and stays constant upon further increase of the coverage (figure 3(d)).

With minor deposition of F_{16}CuPc (1 Å and 2 Å) on Ag(111), shown in figure 3(b), the HOMO-derived peak is centered at 1.30 eV BE and two faint peaks at higher BE are visible. The fine structure in the rather sharp HOMO peak can be assigned to stem from hole-vibration coupling [61] and confirms that the F_{16}CuPc monolayer on Ag(111) is well ordered, as was shown previously by means of scanning tunneling microscopy (STM) [92–94]. With more F_{16}CuPc deposition the intensity of the HOMO peak increases and a small peak near the Fermi edge (0.11 eV), which can be assigned to the F-LUMO, gains intensity and submerges beyond nominal monolayer coverage. Strikingly, for monolayer coverage the formerly faint peak centered at 1.77 eV BE has almost the same intensity as the HOMO-derived peak (at 1.30 eV BE). For multilayer coverage, only one broad peak at 1.94 eV BE is apparent, which is in accordance with previous multilayer F_{16}CuPc/Ag(111) UPS data [95]. Overall, the thickness-dependent evolution of the valence band spectra is similar to F_{16}CuPc/Au(111) [88] and to perfluorinated pentacene/Ag(111) [87] but different to CuPc/Ag(111) [96]. This demonstrates the decisive impact of the intramolecular polar C–F bonds on the electronic structure as will be discussed in more detail further below.

For the heterostructures, TiOPc bilayers on Ag(111) have been prepared by thermal desorption of multilayers (figure S1). The valence band spectra of F_{16}CuPc/TiOPc/Ag(111) are shown in figure 3(c): upon stepwise deposition of F_{16}CuPc the intensity of the TiOPc HOMO-derived peak attenuates gradually and still remains clearly visible for nominal F_{16}CuPc multilayer coverage. The F_{16}CuPc HOMO-derived peak on bilayer TiOPc/Ag(111) is centered at approximately 2.00 eV BE for all thicknesses (from 1 Å to 48 Å). By initial F_{16}CuPc deposition the VL (figure 3(d)) stays constant at 4.32 eV up to a thickness of 4 Å and shifts gradually to 4.51 eV by further F_{16}CuPc deposition.

4. Discussion

In order to discuss the electronic structure of the interfaces according to effects #1 to #6 mentioned in the introduction, we show growth models based on literature data in the top panel of figure 4. In the TiOPc monolayer on Ag(111) the molecules show a TiO-up orientation and form a highly ordered checkerboard structure [11, 97]. The second layer shows a TiO-down orientation [80], which leads to antiparallel molecular dipole moments as shown in figure 4(a); in multilayers also two-dimensional TiO-up and down layer-by-layer formation takes place [81, 83]. For F_{16}CuPc on Ag(111) (figure 4(b)) the molecules adopt a bent conformation in the monolayer, with the central copper atom being located at a lower position and the fluorine atoms being adsorbed at a higher vertical position, as experimentally determined [88, 98] and shown by density functional theory (DFT)-modeling [92]. It is reasonable to believe that the molecules remain in their planar gas phase conformation from the second layer onwards. Furthermore, STM studies indicate a well-ordered monolayer structure with the molecules in the second layer being located at the bridge positions of the first layers and a 45° rotation between the molecular axes [92–94] and STM also indicates layer-by-layer growth of the first and second layers [93]. For the heterostructures, it was shown that fluorinated hexaazatrinaphthylene and perylenetetracarboxylic dianhydride show both an ordered growth on TiOPc layers [99, 100] and we expect that also F_{16}CuPc grows well-ordered on the bi-TiOPc layer.

The UPS and XPS results are schematically summarized with ELDs in the bottom panel of figure 4. In each case, the work function of the Ag(111) substrate as well as the HOMO and F-LUMO level position and the respective core levels (including the different components due to chemical shifts) of the organic layers are displayed. For the single-component systems, the values are taken from the spectra of organic layers with nominal monolayer coverage (QCM thickness: 4 Å), nominal bilayer coverage (QCM thickness: 8 Å) and multilayer coverage (QCM thickness: 64 Å). For the heterostructure, the energy levels of the annealed TiOPc bilayer and these of subsequently deposited F_{16}CuPc layers with QCM thicknesses of 4 Å and 48 Å are shown. In our ELDs we use the peak maxima for valence and core levels, although in literature ELDs often the onset of the HOMO-level is used, as it is the relevant parameter for charge transport and injection [101–103].

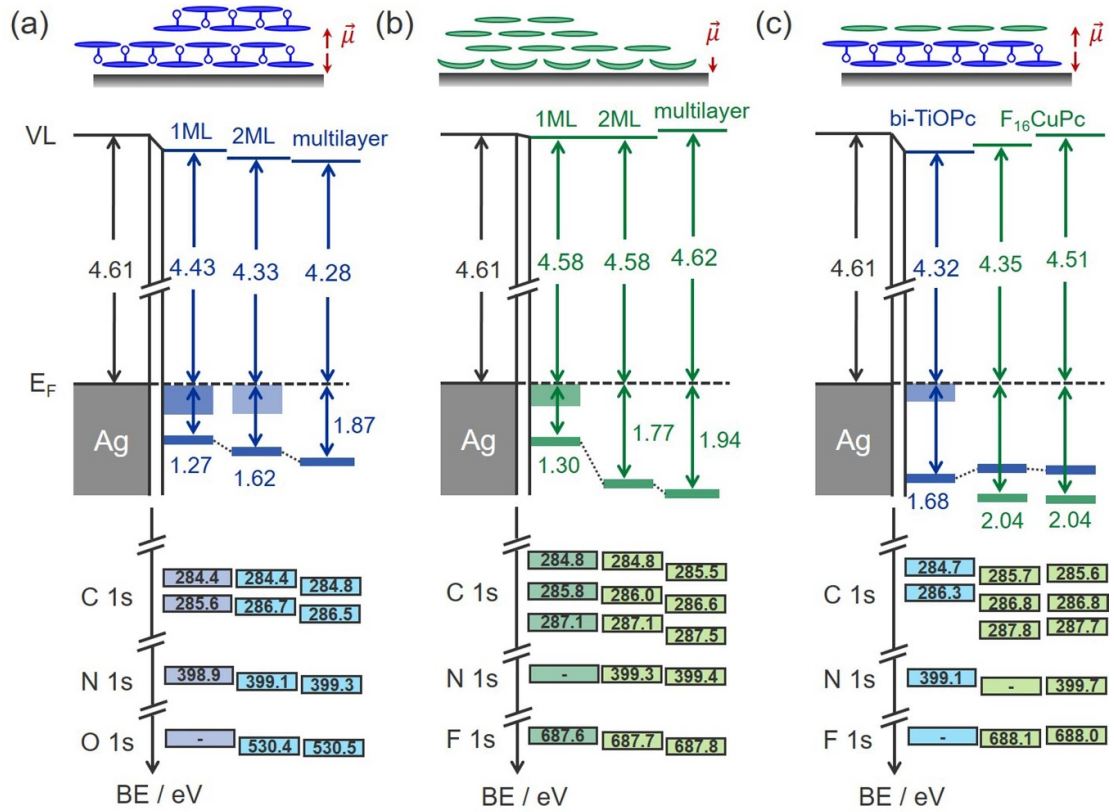

Figure 4. Schematic growth models (top panel) and energy level diagrams (bottom panel) of the investigated thin films. The growth models show side views of the thin films and are based on literature data as described in the text. The energy values of the ELDs are based on the respective peak maxima of our UPS and XPS measurements. In each ELD on the left the Ag(111) substrate with its work function and Fermi-level (E_F) is displayed. For the molecular thin films, the position of the HOMO, the F-LUMO and the core levels are shown. For the single-component systems, monolayer (1 ML), bilayer (2 ML) and multilayer coverage are shown and for the heterostructure monolayer and multilayer F_{16}CuPc on a bilayer TiOPc is shown.

However, the determination of the onset can be ambiguous, in particular if spectral signatures from different layers overlap, e.g. in the spectrum of the 8 Å thick F_{16}CuPc film on Ag(111) in figure 3(b).

The electronic structure of TiOPc deposited on Ag(111) indicates a clear chemisorption behavior (effect #5): the chemical shift between C–C and C–N decreases from 1.55 eV in the multilayer to 1.30 eV in the monolayer, which is a tell-tale sign for chemisorption [18, 38]. Furthermore, the LUMO-derived feature in the monolayer is clearly visible and well below the Fermi-level of the metal substrate. This is due to electron transfer from the substrate into the LUMO. Such a directed charge transfer leads to an interface dipole, which should increase the VL (effect #2) and the dipole layer of the monolayer with TiO-up orientation should additionally increase VL (effect #3). However, the VL decreases by 0.18 eV and it can be concluded that the push-back (effect #1) dominates the position of the VL for monolayer coverage. The subsequent decrease of the VL upon bilayer formation is due to the dipole layer of TiOPc in the TiO-down orientation (effect #3). Notably, this VL-shift does not affect the position of the HOMO-level and the core levels: for the TiO-up orientation the molecular dipole moments are located above the main molecular plane comprising all of the carbon and nitrogen atoms. Consequently, the C 1s and N 1s core levels (and likewise the HOMO-level) are not significantly affected by the molecular dipole layer [40]. For the bilayer system the dipole layers are located between the two molecular main planes and cancel each other. Further deposition of TiOPc leads to a shift to higher BE of both, the valence band and core levels, due to the screening (effect #4) at the organic–metal interface. Overall, even for this structurally well-characterized system [80, 81, 83, 84, 100, 104], a quantitative assignment of the shifts remains challenging, since too many contributions occur concomitantly: the shift of the HOMO between mono- and bilayer has a screening, a chemisorption and a molecular dipole contribution; the VL-shift is affected by the push-back effect, charge transfer and the molecular dipole moments, which first increase (TiO-up) and then decrease (TiO-down) the VL. Furthermore, adsorption induced bond-length changes can alter the molecular dipole moment in the contact layer to a metal substrate [105, 106].

For F_{16}CuPc on Ag(111), as shown in figure 4(b), the VL at the organic–metal interface is affected by the contributions of push-back (effect #1), charge transfer (effect #2) and adsorption induced molecular dipole

moment (effect #3) (the fluorine atoms are 0.20 Å above the carbon atoms [98]). The absence of a notable interface dipole is, most likely, due to a larger net electron transfer from the substrate compared with the TiOPc/Ag(111) system. The monolayer to bilayer BE-shifts of the HOMO-level and the C 1s components (C–C, C–N and C–F) are between 0.4 eV and 0.6 eV and these non-rigid shifts are, again, mainly due to chemisorption (effect #5). Interestingly, the F 1s core level shifts only by 0.1 eV to higher BE, which might be related to the 45° rotation between the molecules in 1 ML and 2 ML [92–94], which affects the electrostatic contribution to polarization (effect #6) in the respective layers. From bilayer to multilayer, the VL stays almost constant and the core levels shift rigidly by 0.1 eV to higher BE while the HOMO-level shift amounts to almost 0.2 eV. These shifts might still have a screening (effect #4) contribution and, furthermore, the molecular packing structure in bilayer and multilayer might be different, which affects the intermolecular polarization (effect #6). The disparity of energy-level shifts measured by UPS and XPS is related to the different information depths: by UPS only the topmost layer is probed while XPS probes almost the entire organic thin film.

For the heterostructure, figure 4(c), the TiOPc layer is obtained by a desorption process, which leads to a well-ordered bilayer [82, 83], which explains the slight difference to the bilayer in figure 4(b). With deposition of F_{16}CuPc molecules the HOMO-level of TiOPc shifts to lower BE, which is due to intermolecular polarization (effect #6). The HOMO-level of F_{16}CuPc is centered at 2.04 eV BE and does not show a thickness-dependent shift. The VL shifts upwards with increasing F_{16}CuPc coverage, which is, most likely, due to pinning of the F_{16}CuPc LUMO-level at E_F [51–54]. Interestingly, despite the absence of charge carriers, Fermi-level pinning can take place at organic–organic interfaces and leads to a potential drop over the contact layer and direct charge transfer from the second layer to the (metal) substrate [32]. The constant HOMO-position and the shifting VL highlight an important difference in VL and valence energy-level determination by UPS for laterally inhomogeneous samples (i.e. F_{16}CuPc islands on the TiOPc layer): for common experimental setups, the VL is the area-averaged mean of local surface potentials (i.e. the covered and uncovered TiOPc-patches), while all valence electron features (i.e. HOMO-levels of F_{16}CuPc and TiOPc) of the probed sample area appear in the spectra [31]. Consequently, great care has to be taken for IE determination and in general thin films with multilayer coverage give the most reliable IEs: the F_{16}CuPc multilayer IEs in the single-component systems (6.56 eV) and the heterostructure (6.55 eV) are virtually identical and in particular the IE in the contact layer to the metal substrate (5.88 eV) is far too low, which is due to the screening effect and the chemisorptive behavior. Notably, F_{16}CuPc does not show such chemisorptive behavior on the TiOPc buffer layer, i.e. this layer actually decouples F_{16}CuPc from Ag(111), and the organic TiOPc layer can be regarded as a dielectric layer. Such spacers change chemisorption-driven fractional charge transfer (partially filled F-LUMO) at the organic–metal interface into electrostatically-driven integer charge transfer across the dielectric layer as was also previously shown using inorganic spacer layers [107, 108].

5. Conclusion

Virtually all optoelectronic applications rely on well-matched energy levels throughout the device structure and ELDs are central to explain device performance. Often literature values are used for ELDs and vacuum-level alignment across all layers is assumed, which, however, is rather the exception than the rule. Consequently, experimental energy-level alignment determination is indispensable for organic device design and our results give guidelines how to interpret XPS and UPS data of organic–metal and organic–organic interfaces. In particular, usually more than one spectrum is necessary to obtain a full picture of interface energetics. For example, at first glance the UPS data of the F_{16}CuPc monolayer on Ag(111) points to weak interaction (due to the constant VL). However, in fact chemisorption involving an organic–metal charge transfer and adsorption induced conformational changes takes place, which is unraveled by additional UPS data and, in particular, by the core-level shifts measured by XPS. In case extensive photoelectron spectroscopy measurements are not possible or literature values are used, multilayer IEs are most suitable for ELDs of device structures.

Data availability statement

All data that support the findings of this study are included within the article (and any supplementary files).

Acknowledgments

Financial support from the National Natural Science Foundation of China (Grant No. 22150610468), the Collaborative Innovation Center of Suzhou Nano Science and Technology (NANO-CIC), the 111 Project of the Chinese State Administration of Foreign Experts Affairs, the Suzhou Key Laboratory of Functional Nano and Soft Materials and the Deutsche Forschungsgemeinschaft (DFG) is gratefully acknowledged. Q W gratefully acknowledges financial support from the China Scholarship Council.

Conflict of interest

The authors declare that they have no known competing financial interests or personal relationships that could have appeared to influence the work reported in this paper.

ORCID iDs

Qi Wang https://orcid.org/0000-0002-9777-3637
Alexander Gerlach https://orcid.org/0000-0003-1787-1868
Frank Schreiber https://orcid.org/0000-0003-3659-6718
Steffen Duhm https://orcid.org/0000-0002-5099-5929

References

[1] Koch N 2021 Opportunities for energy level tuning at inorganic/organic semiconductor interfaces *Appl. Phys. Lett.* **119** 260501
[2] Li P and Lu Z-H 2021 Interface engineering in organic electronics: energy-level alignment and charge transport *Small Sci.* **1** 2000015
[3] Shen D, Chen W-C, Lo M-F and Lee C-S 2021 Charge-transfer complexes and their applications in optoelectronic devices *Mater. Today Energy* **20** 100644
[4] Fahlman M, Fabiano S, Gueskine V, Simon D, Berggren M and Crispin X 2019 Interfaces in organic electronics *Nat. Rev. Mater.* **4** 627–50
[5] Niederhausen J, Mazzio K A and MacQueen R W 2021 Inorganic-organic interfaces in hybrid solar cells *Electron. Struct.* **3** 033002
[6] Athanasopoulos S, Schauer F, Nádaždy V, Weiß M, Kahle F-J, Scherf U, Bässler H and Köhler A 2019 What is the binding energy of a charge transfer state in an organic solar cell? *Adv. Energy Mater.* **9** 1900814
[7] Opitz A *et al* 2022 Thin films of electron donor–acceptor complexes: characterisation of mixed-crystalline phases and implications for electrical doping *Mater. Adv.* **3** 1017–34
[8] Jungbluth A, Kaienburg P and Riede M 2022 Charge transfer state characterization and voltage losses of organic solar cells *J. Phys. Mater.* **5** 024002
[9] Otero R, Vázquez de Parga A L and Gallego J M 2017 Electronic, structural and chemical effects of charge-transfer at organic/inorganic interfaces *Surf. Sci. Rep.* **72** 105–45
[10] Chen M-T *et al* 2019 Energy-level alignment at strongly coupled organic–metal interfaces *J. Phys.: Condens. Matter* **31** 194002
[11] Widdascheck F, Hauke A A and Witte G 2019 A solvent-free solution: vacuum-deposited organic monolayers modify work functions of noble metal electrodes *Adv. Funct. Mater.* **29** 1808385
[12] Koch N, Duhm S, Rabe J P, Vollmer A and Johnson R L 2005 Optimized hole injection with strong electron acceptors at organic-metal interfaces *Phys. Rev. Lett.* **95** 237601
[13] Liu Y *et al* 2022 Recent progress in organic solar cells (part I material science) *Sci. China Chem.* **65** 224–68
[14] Ostroverkhova O 2016 Organic optoelectronic materials: mechanisms and applications *Chem. Rev.* **116** 13279–412
[15] Duhm S 2022 Interface energetics make devices *Electron. Struct.* **4** 034003
[16] Olthof S 2021 The impact of UV photoelectron spectroscopy on the field of organic optoelectronics—a retrospective *Adv. Opt. Mater.* **9** 2100227
[17] Veal T D, Scanlon D O, Kostecki R and Arca E 2021 Accelerating the development of new solar absorbers by photoemission characterization coupled with density functional theory *J. Phys. Energy* **3** 032001
[18] Franco-Cañellas A, Duhm S, Gerlach A and Schreiber F 2020 Binding and electronic level alignment of π-conjugated systems on metals *Rep. Prog. Phys.* **83** 066501
[19] Ishii H, Sugiyama K, Ito E and Seki K 1999 Energy level alignment and interfacial electronic structures at organic/metal and organic/organic interfaces *Adv. Mater.* **11** 605–25
[20] Ogle J, Powell D, Flannery L and Whittaker-Brooks L 2021 Interplay between morphology and electronic structure in emergent organic and π-d conjugated organometal thin film materials *Ind. Eng. Chem. Res.* **60** 15365–79
[21] Hofmann A, Schmid M and Brütting W 2021 The many facets of molecular orientation in organic optoelectronics *Adv. Opt. Mater.* **9** 2101004
[22] Kraut E A, Grant R W, Waldrop J R and Kowalczyk S P 1980 Precise determination of the valence-band edge in x-ray photoemission spectra: application to measurement of semiconductor interface potentials *Phys. Rev. Lett.* **44** 1620–3
[23] Himpsel F J, Hollinger G and Pollak R A 1983 Determination of the Fermi-level pinning position at Si(111) surfaces *Phys. Rev.* B **28** 7014–8
[24] Travnikova O, Børve K J, Patanen M, Söderström J, Miron C, Sæthre L J, Mårtensson N and Svensson S 2012 The ESCA molecule—historical remarks and new results *J. Electron Spectrosc. Relat. Phenom.* **185** 191–7
[25] Regoutz A, Wolinska M S, Fernando N K and Ratcliff L E 2020 A combined density functional theory and x-ray photoelectron spectroscopy study of the aromatic amino acids *Electron. Struct.* **2** 044005
[26] Seah M P and Dench W A 1979 Quantitative electron spectroscopy of surfaces: a standard data base for electron inelastic mean free paths in solids *Surf. Interface Anal.* **1** 2–11

[27] Nakayama Y, Kera S and Ueno N 2020 Photoelectron spectroscopy on single crystals of organic semiconductors: experimental electronic band structure for optoelectronic properties *J. Mater. Chem.* C **8** 9090–132
[28] Cahen D and Kahn A 2003 Electron energetics at surfaces and interfaces: concepts and experiments *Adv. Mater.* **15** 271–7
[29] Schultz T, Lenz T, Kotadiya N, Heimel G, Glasser G, Berger R, Blom P W M, Amsalem P, de Leeuw D M and Koch N 2017 Reliable work function determination of multicomponent surfaces and interfaces: the role of electrostatic potentials in ultraviolet photoelectron spectroscopy *Adv. Mater. Interfaces* **4** 1700324
[30] Koller G, Winter B, Oehzelt M, Ivanco J, Netzer F P and Ramsey M G 2007 The electronic band alignment on nanoscopically patterned substrates *Org. Electron.* **8** 63–68
[31] Schultz T, Amsalem P, Kotadiya N B, Lenz T, Blom P W M and Koch N 2019 Importance of substrate work function homogeneity for reliable ionization energy determination by photoelectron spectroscopy *Phys. Status Solidi* b **256** 1800299
[32] Oehzelt M, Akaike K, Koch N and Heimel G 2015 Energy-level alignment at organic heterointerfaces *Sci. Adv.* **1** e1501127
[33] Taucher T C, Hehn I, Hofmann O T, Zharnikov M and Zojer E 2016 Understanding chemical versus electrostatic shifts in x-ray photoelectron spectra of organic self-assembled monolayers *J. Phys. Chem.* C **120** 3428–37
[34] Frericks M, Pflumm C, Mankel E, Mayer T and Jaegermann W 2021 Space charge regions at organic p-i-homointerfaces from advanced modeling of *in situ*-prepared interfaces analyzed by photoelectron spectroscopy *ACS Appl. Electron. Mater.* **3** 1211–27
[35] Nakayama Y, Uragami Y, Yamamoto M, Yonezawa K, Mase K, Kera S, Ishii H and Ueno N 2016 High-resolution core-level photoemission measurements on the pentacene single crystal surface assisted by photoconduction *J. Phys.: Condens. Matter* **28** 094001
[36] Franco-Cañellas A, Wang Q, Broch K, Duncan D A, Thakur P K, Liu L, Kera S, Gerlach A, Duhm S and Schreiber F 2017 Metal-organic interface functionalization via acceptor end groups: PTCDI on coinage metals *Phys. Rev. Mater.* **1** 013001
[37] Tseng T-C *et al* 2010 Charge-transfer-induced structural rearrangements at both sides of organic/metal interfaces *Nat. Chem.* **2** 374–9
[38] Heimel G *et al* 2013 Charged and metallic molecular monolayers through surface-induced aromatic stabilization *Nat. Chem.* **5** 187–94
[39] Willenbockel M, Lüftner D, Stadtmüller B, Koller G, Kumpf C, Soubatch S, Puschnig P, Ramsey M G and Tautz F S 2015 The interplay between interface structure, energy level alignment and chemical bonding strength at organic–metal interfaces *Phys. Chem. Chem. Phys.* **17** 1530–48
[40] Zojer E, Taucher T C and Hofmann O T 2019 The impact of dipolar layers on the electronic properties of organic/inorganic hybrid interfaces *Adv. Mater. Interfaces* **6** 1900581
[41] D'Avino G, Duhm S, Della Valle R G, Heimel G, Oehzelt M, Kera S, Ueno N, Beljonne D and Salzmann I 2020 Electrostatic interactions shape molecular organization and electronic structure of organic semiconductor blends *Chem. Mater.* **32** 1261–71
[42] Witte G, Lukas S, Bagus P S and Wöll C 2005 Vacuum level alignment at organic/metal junctions: 'Cushion' effect and the interface dipole *Appl. Phys. Lett.* **87** 263502
[43] Romaner L, Heimel G, Brédas J-L, Gerlach A, Schreiber F, Johnson R L, Zegenhagen J, Duhm S, Koch N and Zojer E 2007 Impact of bidirectional charge transfer and molecular distortions on the electronic structure of a metal-organic interface *Phys. Rev. Lett.* **99** 256801
[44] Natan A, Kronik L, Haick H and Tung R T 2007 Electrostatic properties of ideal and non-ideal polar organic monolayers: implications for electronic devices *Adv. Mater.* **19** 4103–17
[45] Fukagawa H, Hosoumi S, Yamane H, Kera S and Ueno N 2011 Dielectric properties of polar-phthalocyanine monolayer systems with repulsive dipole interaction *Phys. Rev.* B **83** 085304
[46] Aihara T, Abd-Rahman S A and Yoshida H 2021 Metal screening effect on energy levels at metal/organic interface: precise determination of screening energy using photoelectron and inverse-photoelectron spectroscopies *Phys. Rev.* B **104** 085305
[47] Hill I G, Mäkinen A J and Kafafi Z H 2000 Initial stages of metal/organic semiconductor interface formation *J. Appl. Phys.* **88** 889–95
[48] Yamada K, Yanagisawa S, Koganezawa T, Mase K, Sato N and Yoshida H 2018 Impact of the molecular quadrupole moment on ionization energy and electron affinity of organic thin films: experimental determination of electrostatic potential and electronic polarization energies *Phys. Rev.* B **97** 245206
[49] Sato N, Seki K and Inokuchi H 1981 Polarization energies of organic solids determined by ultraviolet photoelectron spectroscopy *J. Chem. Soc. Faraday Trans.* **2, 77** 1621–33
[50] Tsiper E V and Soos Z G 2003 Electronic polarization in pentacene crystals and thin films *Phys. Rev.* B **68** 085301
[51] Oehzelt M, Koch N and Heimel G 2014 Organic semiconductor density of states controls the energy level alignment at electrode interfaces *Nat. Commun.* **5** 4174
[52] Yang J-P, Bussolotti F, Kera S and Ueno N 2017 Origin and role of gap states in organic semiconductor studied by UPS: as the nature of organic molecular crystals *J. Phys. D: Appl. Phys.* **50** 423002
[53] Zhai T, Wang R, Katase T, Quigley F, Ohta H, Amsalem P, Koch N and Duhm S 2020 Substrate-independent energy-level pinning of an organic semiconductor providing versatile hole-injection electrodes *ACS Appl. Electron. Mater.* **2** 3994–4001
[54] Hagenlocher J, Broch K, Zwadlo M, Lepple D, Rawle J, Carla F, Kera S, Schreiber F and Hinderhofer A 2022 Thickness-dependent energy-level alignment at the organic–organic interface induced by templated gap states *Adv. Mater. Interfaces* **9** 2101382
[55] Sueyoshi T, Fukagawa H, Ono M, Kera S and Ueno N 2009 Low-density band-gap states in pentacene thin films probed with ultrahigh-sensitivity ultraviolet photoelectron spectroscopy *Appl. Phys. Lett.* **95** 183303
[56] Bussolotti F 2015 High-sensitivity ultraviolet photoemission spectroscopy technique for direct detection of gap states in organic thin films *J. Electron Spectrosc. Relat. Phenom.* **204** 29–38
[57] Ueno N and Kera S 2008 Electron spectroscopy of functional organic thin films: deep insights into valence electronic structure in relation to charge transport property *Prog. Surf. Sci.* **83** 490–557
[58] Koller G, Berkebile S, Oehzelt M, Puschnig P, Ambrosch-Draxl C, Netzer F P and Ramsey M G 2007 Intra- and intermolecular band dispersion in an organic crystal *Science* **317** 351–5
[59] Hammer B 2006 Special sites at noble and late transition metal catalysts *Top. Catal.* **37** 3–16
[60] Kera S, Hosokai T and Duhm S 2018 Characteristics of organic–metal interaction: a perspective from bonding distance to orbital delocalization *J. Phys. Soc. Japan* **87** 061008
[61] Kera S, Yamane H and Ueno N 2009 First-principles measurements of charge mobility in organic semiconductors: valence hole–vibration coupling in organic ultrathin films *Prog. Surf. Sci.* **84** 135–54
[62] Duhm S, Xin Q, Hosoumi S, Fukagawa H, Sato K, Ueno N and Kera S 2012 Charge reorganization energy and small polaron binding energy of rubrene thin films by ultraviolet photoelectron spectroscopy *Adv. Mater.* **24** 901–5

[63] Puschnig P, Berkebile S, Fleming A J, Koller G, Emtsev K, Seyller T, Riley J D, Ambrosch-Draxl C, Netzer F P and Ramsey M G 2009 Reconstruction of molecular orbital densities from photoemission data *Science* **326** 702
[64] Dauth M, Graus M, Schelter I, Wießner M, Schöll A, Reinert F and Kümmel S 2016 Perpendicular emission, dichroism, and energy dependence in angle-resolved photoemission: the importance of the final state *Phys. Rev. Lett.* **117** 183001
[65] Haags A *et al* 2022 Momentum space imaging of σ orbitals for chemical analysis *Sci. Adv.* **8** eabn0819
[66] Woodruff D P and Bradshaw A M 1994 Adsorbate structure determination on surfaces using photoelectron diffraction *Rep. Prog. Phys.* **57** 1029–80
[67] Fedchenko O, Winkelmann A and Schönhense G 2022 Structure analysis using time-of-flight momentum microscopy with hard x-rays: status and prospects *J. Phys. Soc. Japan* **91** 091006
[68] Borghetti P, El-Sayed A, Goiri E, Rogero C, Lobo-Checa J, Floreano L, Ortega J E and de Oteyza D G 2014 Spectroscopic fingerprints of work-function-controlled phthalocyanine charging on metal surfaces *ACS Nano* **8** 12786–95
[69] Peisert H, Kolacyak D and Chassé T 2009 Site-specific charge-transfer screening at organic/metal interfaces *J. Phys. Chem.* C **113** 19244–50
[70] Wang L, Chen W and Wee A T S 2008 Charge transfer across the molecule/metal interface using the core hole clock technique *Surf. Sci. Rep.* **63** 465–86
[71] Deleuze M S, Trofimov A B and Cederbaum L S 2001 Valence one-electron and shake-up ionization bands of polycyclic aromatic hydrocarbons. I. Benzene, naphthalene, anthracene, naphthacene, and pentacene *J. Chem. Phys.* **115** 5859–82
[72] Rocco M L M, Haeming M, Batchelor D R, Fink R, Schöll A and Umbach E 2008 Electronic relaxation effects in condensed polyacenes: a high-resolution photoemission study *J. Chem. Phys.* **129** 074702
[73] Major G H, Fairley N, Sherwood P M A, Linford M R, Terry J, Fernandez V and Artyushkova K 2020 Practical guide for curve fitting in x-ray photoelectron spectroscopy *J. Vac. Sci. Technol.* A **38** 061203
[74] Isaacs M A, Davies-Jones J, Davies P R, Guan S, Lee R, Morgan D J and Palgrave R 2021 Advanced XPS characterization: XPS-based multi-technique analyses for comprehensive understanding of functional materials *Mater. Chem. Front.* **5** 7931–63
[75] Greczynski G and Hultman L 2022 A step-by-step guide to perform x-ray photoelectron spectroscopy *J. Appl. Phys.* **132** 011101
[76] Ishii H, Kudo K, Nakayama T and Ueno N 2015 *Electronic Processes in Organic Electronics* (Tokyo: Springer) (https://doi.org/10.1007/978-4-431-55206-2)
[77] Suga S, Sekiyama A and Tusche C 2021 *Photoelectron Spectroscopy* (Cham: Springer) (https://doi.org/10.1007/978-3-030-64073-6)
[78] Kuzumoto Y, Matsuyama H and Kitamura M 2013 Partially fluorinated copper phthalocyanine toward band engineering for high-efficiency organic photovoltaics *Jpn. J. Appl. Phys.* **53** 01AB03
[79] Peisert H, Uihlein J, Petraki F and Chassé T 2015 Charge transfer between transition metal phthalocyanines and metal substrates: the role of the transition metal *J. Electron Spectrosc. Relat. Phenom.* **204** 49–60
[80] Kröger I, Stadtmüller B and Kumpf C 2016 Submonolayer and multilayer growth of titaniumoxide-phthalocyanine on Ag(111) *New J. Phys.* **18** 113022
[81] Fernandez L, Thussing S, Mänz A, Sundermeyer J, Witte G and Jakob P 2017 The discrete nature of inhomogeneity: the initial stages and local configurations of TiOPc during bilayer growth on Ag(111) *Phys. Chem. Chem. Phys.* **19** 2495–502
[82] Kera S, Yabuuchi Y, Yamane H, Setoyama H, Okudaira K K, Kahn A and Ueno N 2004 Impact of an interface dipole layer on molecular level alignment at an organic-conductor interface studied by ultraviolet photoemission spectroscopy *Phys. Rev.* B **70** 085304
[83] Kothe M, Widdascheck F and Witte G 2019 Titanylphthalocyanine films on Ag(111): an epitaxial metal/organic heterosystem with an exceptional smooth surface *J. Phys. Chem.* C **123** 6097–106
[84] Lerch A *et al* 2017 Electronic structure of titanylphthalocyanine layers on Ag(111) *J. Phys. Chem.* C **121** 25353–63
[85] Yang J, Wang Q, Wan S, Wu D, Chen M, Kashtanov S and Duhm S 2021 Photoelectron spectroscopy reveals molecular diffusion through physisorbed template layers on Au(111) *Electron. Struct.* **3** 024002
[86] Greulich K, Belser A, Basova T, Chassé T and Peisert H 2022 Interfaces between different iron phthalocyanines and Au(111): influence of the fluorination on structure and interfacial interactions *J. Phys. Chem.* C **126** 716–27
[87] Duhm S *et al* 2010 Influence of intramolecular polar bonds on interface energetics in perfluoro-pentacene on Ag(111) *Phys. Rev.* B **81** 045418
[88] Wang Q, Franco-Cañellas A, Yang J, Hausch J, Struzek S, Chen M, Thakur P K, Gerlach A, Duhm S and Schreiber F 2020 Heteromolecular bilayers on a weakly interacting substrate: physisorptive bonding and molecular distortions of copper–hexadecafluorophthalocyanine *ACS Appl. Mater. Interfaces* **12** 14542–51
[89] Abd-Rahman S A, Yamaguchi T, Kera S and Yoshida H 2022 Sample-shape dependent energy levels in organic semiconductors *Phys. Rev.* B **106** 075303
[90] Lu M-C, Wang R-B, Yang A and Duhm S 2016 Pentacene on Au(1 1 1), Ag(1 1 1) and Cu(1 1 1): from physisorption to chemisorption *J. Phys.: Condens. Matter* **28** 094005
[91] Wang C, Niu D, Zhao Y, Wang S, Qian C, Huang H, Xie H and Gao Y 2019 Interface energy-level alignment between black phosphorus and F16CuPc molecular films *J. Phys. Chem.* C **123** 10443–50
[92] Chen L, Li H and Wee A T S 2009 Nonlocal chemical reactivity at organic−metal interfaces *ACS Nano* **3** 3684–90
[93] Huang H, Chen W and Wee A T S 2008 Low-temperature scanning tunneling microscopy investigation of epitaxial growth of F_{16}CuPc thin films on Ag(111) *J. Phys. Chem.* C **112** 14913–8
[94] Kleimann C, Stadtmüller B, Schröder S and Kumpf C 2014 Electrostatic interaction and commensurate registry at the heteromolecular F_{16}CuPc–CuPc interface *J. Phys. Chem.* C **118** 1652–60
[95] Akaike K, Koch N, Heimel G and Oehzelt M 2015 The impact of disorder on the energy level alignment at molecular donor–acceptor interfaces *Adv. Mater. Interfaces* **2** 1500232
[96] Wang Q *et al* 2018 Bilayer formation vs molecular exchange in organic heterostructures: strong impact of subtle changes in molecular structure *J. Phys. Chem.* C **122** 9480–90
[97] Zhao W, Zhu H, Song H, Liu J, Chen Q, Wang Y and Wu K 2018 Adsorption and assembly of photoelectronic TiOPc molecules on coinage metal surfaces *J. Phys. Chem.* C **122** 7695–701
[98] Gerlach A, Schreiber F, Sellner S, Dosch H, Vartanyants I A, Cowie B C C, Lee T L and Zegenhagen J 2005 Adsorption-induced distortion of F_{16}CuPc on Cu(111) and Ag(111): an x-ray standing wave study *Phys. Rev.* B **71** 205425
[99] Hwang H U, Yang S and Kim J W 2020 Interface charge transfer between metal phthalocyanine and fluorinated hexaazatrinaphthylene molecules *Curr. Appl. Phys.* **20** 841–5
[100] Thussing S, Fernández L and Jakob P 2019 Thermal stability and interlayer exchange processes in heterolayers of TiOPc and PTCDA on Ag(1 1 1) *J. Phys.: Condens. Matter* **31** 134002

[101] Jung S, Kim C-H, Bonnassieux Y and Horowitz G 2015 Injection barrier at metal/organic semiconductor junctions with a Gaussian density-of-states *J. Phys. D: Appl. Phys.* **48** 395103
[102] Nakayama Y, Sudo K, Ohashi N, Kera S and Watanabe Y 2021 Interface electronic structure and valence band dispersion of bis(1,2,5-thiadiazolo)-p-quinobis(1,3-dithiole) on polycrystalline Au electrodes *Electron. Struct.* **3** 024006
[103] Chen B, Hu J, Wang Q and Duhm S 2022 Energetic disorder impacts energy-level alignment of alpha-sexithiophene on hydrogen-terminated silicon and silicon oxide *Mater. Res. Express* **9** 085101
[104] Liu X, Wei Y, Reutt-Robey J E and Robey S W 2014 Dipole–dipole interactions in TiOPc adlayers on Ag *J. Phys. Chem.* C **118** 3523–32
[105] Gerlach A, Hosokai T, Duhm S, Kera S, Hofmann O T, Zojer E, Zegenhagen J and Schreiber F 2011 Orientational ordering of nonplanar phthalocyanines on Cu(111): strength and orientation of the electric dipole moment *Phys. Rev. Lett.* **106** 156102
[106] Huang Y L, Chen W, Bussolotti F, Niu T C, Wee A T S, Ueno N and Kera S 2013 Impact of molecule-dipole orientation on energy level alignment at the submolecular scale *Phys. Rev.* B **87** 085205
[107] Hofmann O T, Rinke P, Scheffler M and Heimel G 2015 Integer versus fractional charge transfer at metal(/insulator)/organic interfaces: Cu(/NaCl)/TCNE *ACS Nano* **9** 5391–404
[108] Hollerer M, Lüftner D, Hurdax P, Ules T, Soubatch S, Tautz F S, Koller G, Puschnig P, Sterrer M and Ramsey M G 2017 Charge transfer and orbital level alignment at inorganic/organic interfaces: the role of dielectric interlayers *ACS Nano* **11** 6252–60